Volume 44 | Number 46 | 14 December 2015 | Pages 19735–20268

Dalton Transactions

An international journal of inorganic chemistry

www.rsc.org/dalton

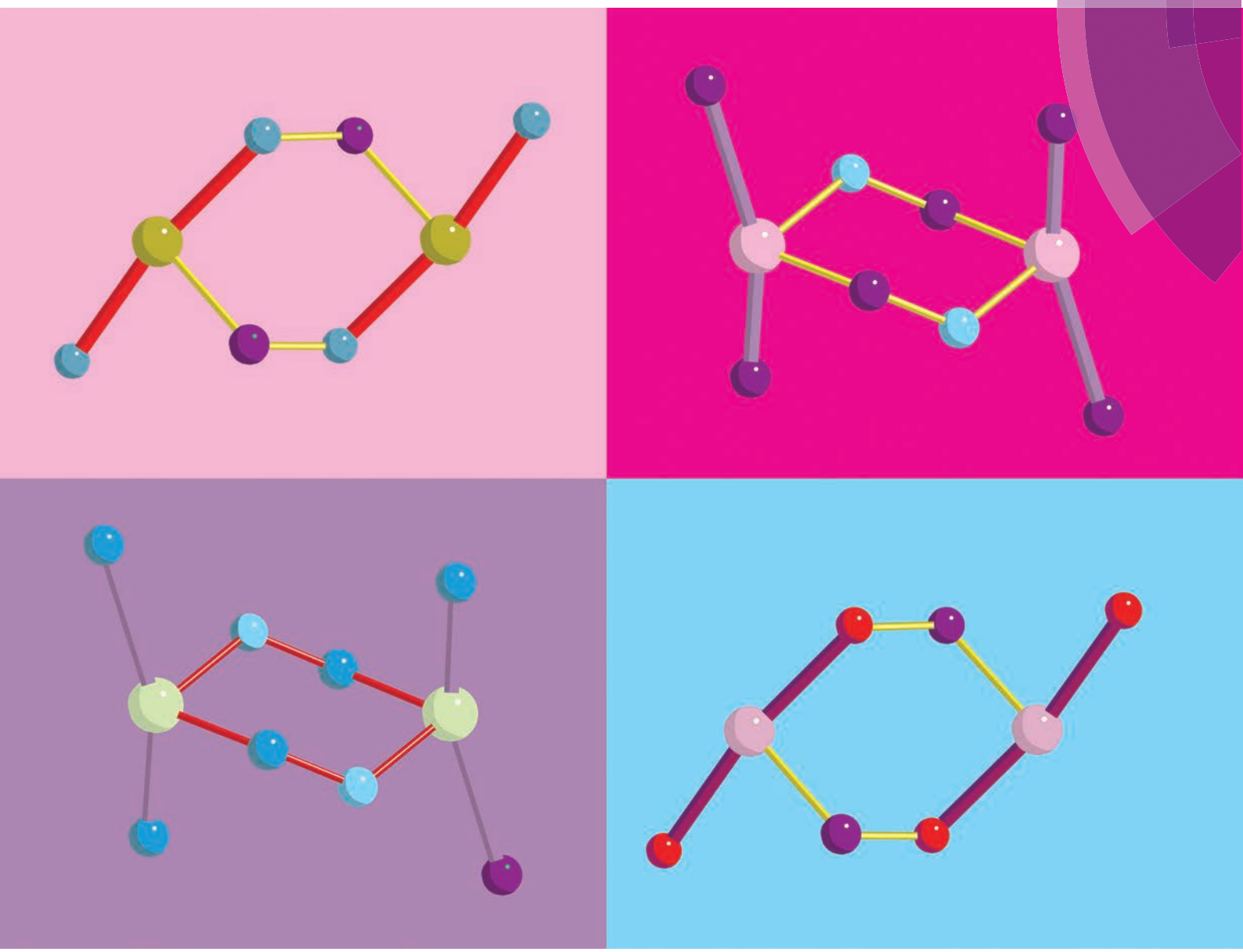

ISSN 1477-9226

ROYAL SOCIETY OF CHEMISTRY

PAPER

Gopalan Rajaraman, Euan K. Brechin *et al.*

Switching the orientation of Jahn–Teller axes in oxime-based Mn^{III} dimers and its effect upon magnetic exchange: a combined experimental and theoretical study

Dalton Transactions

PAPER

View Article Online
View Journal | View Issue

Cite this: *Dalton Trans.*, 2015, **44**, 19805

Switching the orientation of Jahn–Teller axes in oxime-based Mn^{III} dimers and its effect upon magnetic exchange: a combined experimental and theoretical study†

Priyanka Comar,[a] Thayalan Rajeshkumar,[b] Gary S. Nichol,[a] Mateusz B. Pitak,[c] Simon J. Coles,[c] Gopalan Rajaraman*[b] and Euan K. Brechin*[a]

Received 15th September 2015,
Accepted 7th October 2015

DOI: 10.1039/c5dt03615a

www.rsc.org/dalton

A family of Mn^{III} dimers of general formula $[Mn^{III}_2(R\text{-}sao)_2(dpa)_2](ClO_4)_2$ (**1–5**) has been synthesised using derivatised phenolic oximes (R-saoH_2, where R = H, Me, Et, Ph) in combination with di-(2-picolyl)-amine (dpa). Their structures reveal a double-oxime bridged $[Mn^{III}(NO)]_2$ magnetic core in which the Jahn–Teller axes lie perpendicular to the bridging plane, in contrast to two previously reported family members (**6**, **7**). The switch in the orientation of the Jahn–Teller axes is enforced through the use of the chelating ligand which is present in **1–5** and absent in **6–7**. Dc magnetic susceptibility measurements reveal that the exchange interactions between the Mn^{III} metal centres in **1–5** are antiferromagnetic in contrast to that observed for **6** and **7** which are ferromagnetic. DFT calculations performed on complexes **1–6** reproduce both the sign and strength of the *J* values found experimentally. Molecular orbital analysis unlocks a common mechanism of magnetic coupling based upon the orientation of the Jahn–Teller axis, with the magneto-structural correlation also dependent upon the Mn–N–O–Mn angles – with ferromagnetic interactions at smaller dihedral angles.

Introduction

Molecular magnets – molecules containing exchange-coupled paramagnetic metal ions – are an enormously important class of material with potential application across a diverse range of fields from information storage, quantum computation and molecular spintronics to cryogenic refrigeration and biomedical imaging.[1–5] Such species combine the macroscopic properties of magnets with the quantum mechanical properties of molecules, allowing detailed study of quantum size effects in monodisperse, reproducible, orientable, chemically tuneable molecules.[6] Recent years have witnessed a plethora of important scientific breakthroughs including the observation of quantum tunnelling of the magnetization, quantum phase interference, memory effects at T = 14 K, single-molecule magnetic detection, the construction of molecular spintronic devices, molecules and coordination polymers displaying enormously enhanced magnetocaloric effects, and the development of protocols for molecule-based quantum information processing.[7–20] The discovery of such phenomena, and any potential exploitation thereof, is based upon a detailed understanding of, and subsequent control over, the structure–magnetism relationship. This in turn is derived from a systematic synthetic study of the effects of ligand design, metal identity and reaction conditions upon symmetry and structure, in tandem with detailed physical characterisation and theoretical analysis.[21]

Manganese is often a good choice for constructing such molecules: it commonly exists in the II+, III+ and IV+ oxidation states, resulting in the majority of clusters being mixed-valent, which, in turn, decreases the likelihood of antiferromagnetically coupled cages possessing diamagnetic spin ground states.[6] The Jahn–Teller distorted Mn^{III} ion also provides a source magnetic anisotropy that has often been employed in the construction of Single-Molecule Magnets (SMMs),[6] whilst the isotropic Mn^{II} ion finds application in clusters displaying an enhanced magnetocaloric effect (MCE), a phenomenon that can be exploited for low temperature cooling.[17] Application first requires the development of magneto-structural

[a]*EaStCHEM School of Chemistry, The University of Edinburgh, David Brewster Road, Edinburgh, EH9 3FJ Scotland, UK. E-mail: E.Brechin@ed.ac.uk; Tel: +44 (0)131-650-7545*
[b]*Department of Chemistry, Indian Institute of Technology Bombay, Mumbai, 400076, India. E-mail: rajaraman@chem.iitb.ac.in*
[c]*UK National Crystallographic Service, Chemistry, University of Southampton, Southampton, Highfield Campus, SO17 1BJ, UK*

†Electronic supplementary information (ESI) available: Full synthetic and crystallographic details; packing diagrams, additional magnetic data and details of the DFT calculations. CCDC 1044300–1044304. For ESI and crystallographic data in CIF or other electronic format see DOI: 10.1039/c5dt03615a

correlations, but this can often be a difficult task due to prohibitively large nuclearities and/or complex exchange interaction patterns. One way to overcome such issues is to construct families of low nuclearity cages (*e.g.* dimers, trimers, tetramers) which mimic the building blocks of the bigger cages, and investigate how small structural perturbations affect magnetic exchange. Detailed studies on Mn^{III} dimers, however, remain relatively scarce.[22] A recent experimental and theoretical study of alkoxide-bridged $[Mn^{III}(OR)]_2$ dimers revealed that the dominant structural feature controlling magnetic exchange (J) was the relative orientations of the Jahn–Teller axes.[22] A parallel orientation, perpendicular to the bridging plane of the molecule (**Type I**, Fig. 1) resulted in weak antiferromagnetic exchange; a parallel orientation within the bridging plane (**Type II**, Fig. 1) led to borderline cases in which the exchange could be either weakly ferromagnetic or weakly antiferromagnetic; whilst a perpendicular orientation (**Type III**, Fig. 1) produced ferromagnetic exchange. For the oxime/oxo bridged species $[Mn^{III}_2(O)(NO)]$ (Fig. 1, **A**) the Mn–N–O–Mn torsion angle dominates, with a linear correlation found between the magnitude of J and the torsion angle.[22] DFT studies on double-oxime bridged dimers $[Mn^{III}(NO)]_2$ (Fig. 1, **B**) also revealed a pronounced dependence of the exchange coupling on the relative twisting of the oxime moiety, as proposed previously in more complicated $[Mn^{III}_3]$ and $[Mn^{III}_6]$ clusters,[23] resulting from an accidental orthogonality between the Mn–N–O plane of the first Mn^{III} ion and the Jahn–Teller axis of the second Mn^{III} ion.[22]

In order to extend the family of double-oxime bridged Mn^{III} dimers – which has just two members – we herein report a series of double-oxime bridged $[Mn^{III}(NO)]_2$ species in which employment of the chelating ligand di-(2-picolyl)-amine, dpa (Fig. 2), switches the orientation of the Jahn–Teller axes from being in the bridging plane (structure type **B**, Fig. 1) to being perpendicular to the bridging plane (structure type **C**, Fig. 1) and present a combined experimental and theoretical analyses of the effect of this Jahn–Teller switching upon the magnetic exchange between the two Mn^{III} ions.

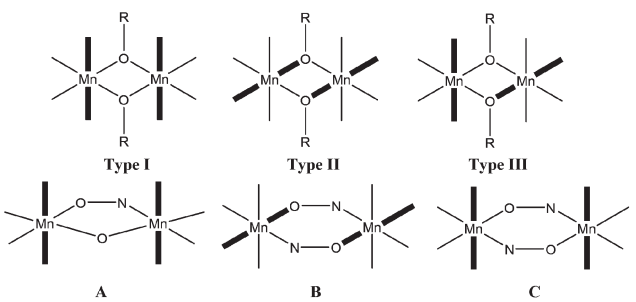

Fig. 1 Top: alkoxide bridged dimers $[Mn^{III}(OR)]_2$ with **Type I–III** structures differing in the relative orientations of the Jahn–Teller axes, which are highlighted in bold. Bottom: oxime/oxo dimers $[Mn^{III}_2(O)(NO)]$ (**A**), and the double oxime bridged dimers $[Mn^{III}(NO)]_2$ in which the Jahn–Teller axes lie in the bridging plane (**B**), and perpendicular to the bridging plane (**C**).

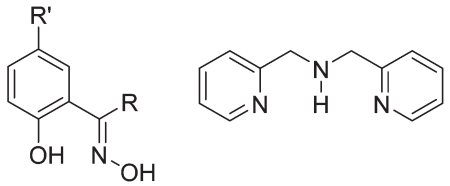

Fig. 2 Left: generic structure of a phenolic oxime. $saoH_2$, R = R′ = H; Me-$saoH_2$, R = Me, R′ = H, Et-$saoH_2$, R = Et, R′ = H; Ph-$saoH_2$, R = Ph, R′ = H; Me_2-$saoH_2$, R = R′ = Me. Right: di-(2-picolyl)-amine, dpa.

Experimental

Materials and physical measurements

All synthetic procedures were performed under aerobic conditions using chemicals as received (reagent grade). **Caution!** Although no problems were encountered here, care should be taken when handling the potentially explosive perchlorate anion. The substituted phenolic oximes were synthesised using the appropriate precursor ketones, hydroxylamine hydrochloride and sodium acetate in EtOH, as described in the literature.[24] Variable temperature, solid state magnetic susceptibility data down to 5 K were collected on a Quantum Design MPMS XL SQUID magnetometer equipped with a 7 T dc magnet. Diamagnetic corrections were applied to the observed paramagnetic susceptibilities using Pascal's constants.

Synthesis

General procedure for the synthesis of $[Mn^{III}_2(R\text{-}sao)_2(dpa)_2](ClO_4)_2$: $Mn(ClO_4)_2{\cdot}6H_2O$ (0.4 mmol) and the appropriate phenolic oxime (0.4 mmol) were dissolved in MeOH (10 mL). NH_4OH (1.6 mmol) was then added to the solution and the reaction left to stir for 40 minutes at room temperature. dpa (0.4 mmol) in EtOH (10 mL) was added to the reaction mixture, which was then filtered after 5 minutes of additional stirring. The black mother liquor was left to evaporate over a period of 4 days, during which time black block-like crystals grew in varying yields. See the ESI† for full synthetic details.

X-Ray crystallography

Diffraction data for samples **1** and **3–5** (CCDC numbers 1044300, 1044302–1044304) were collected on an Oxford Diffraction SuperNova diffractometer using Mo or Cu Kα radiation. The crystal temperature was maintained at 120 K using an Oxford Cryosystems Cryostream 700+ low temperature device. The structures were solved by direct methods and refined by full-matrix least-squares techniques on F^2 using the programs SHELXL[25a] and Olex2.[25b] X-ray data for complex **2** (CCDC 1044301) were collected at 100 K (Oxford Cryosystems Cobra) on a Rigaku AFC12 goniometer equipped with an enhanced sensitivity (HG) Saturn724+ detector mounted at the window of an FR-E+ SuperBright molybdenum rotating anode genera-

tor with VHF Varimax optics (70 m focus). The crystal structure was solved by charge flipping methods in SUPERFLIP[25c] and the full-matrix least-squares refinement on F_o^2 was carried out using SHELXL.[25a] All non-hydrogen atoms were refined with anisotropic displacement parameters. All hydrogen atoms were added at calculated positions and refined using a riding model with isotropic displacement parameters based on the equivalent isotropic displacement parameter (U_{eq}) of the parent atom. Table S1 in the ESI† contains a summary of the experimental crystallographic parameters.

Computational details

Calculations were performed on the full crystal structures of **1–6**. A hybrid B3LYP[26] functional with TZV basis set[27] was employed for calculating the exchange constants as implemented in the G09[28] suite of programs. The high spin states (E-HS) and low spin states (E-BS) were estimated using single determinant wave functions and the broken symmetry approach,[29] respectively, and the corresponding J values were computed from the difference between E-HS and E-BS. Further details about the computational methodology are discussed elsewhere.[30]

Results and discussion

Reacting $Mn(ClO_4)_2{\cdot}6H_2O$ with the appropriate phenolic oxime (R-saoH$_2$, Fig. 2) and the tridentate ligand dpa in alcohol and in the presence of an appropriate base, produces black crystals of the complexes $[Mn_2^{III}(Et\text{-}sao)_2(dpa)_2](ClO_4)_2$ (**1**), $[Mn_2^{III}(Me\text{-}sao)_2(dpa)_2](ClO_4)_2$ (**2**), $[Mn_2^{III}(Me_2\text{-}sao)_2(dpa)_2](ClO_4)_2$ (**3**), $[Mn_2^{III}(sao)_2(dpa)_2](ClO_4)_2$ (**4**), and $[Mn_2^{III}(Ph\text{-}sao)_2(dpa)_2](ClO_4)_2$ (**5**) in varying yields over 4 days.

Complexes **1–5** (Fig. 3 shows representative example **2**, Table S2† pertinent bond lengths and Table 1 magneto-structural data) describe simple, double-oxime bridged $[Mn^{III}(NO)]_2$ dimers with Mn–O–N–Mn torsion angles of approximately 79° (**1**), 62° (**2**), 75° (**3**), 51° (**4**) and 63° (**5**). The remaining coordination sites on each Mn ion are occupied by the three N-atoms of the chelating dpa ligand, and a terminally bonded phenolic O-atom. The metal is thus six coordinate and in a distorted octahedral geometry with the Jahn–Teller axis being the N(pyridine)–Mn–N(pyridine) vector, which lies approximately perpendicular to the bridging $[Mn(NO)]_2$ plane (structure type **C**, Fig. 1). The two Jahn–Teller axes are not strictly co-parallel but lie at dihedral angles (JT–Mn–Mn–JT) of approximately 26° (**1**), 24° (**2**), 21° (**3**), 23° (**4**) and 16° (**5**). The cluster is a 2+ cation with charge balance being maintained through the presence of two ClO_4^- anions (the packing of the molecules in **1–5** is described in the ESI, Fig. S1–S5†). Complexes **1–5** therefore represent an extension to the family of two previously reported $[Mn(NO)]_2$ dimers, namely the complexes $[Mn_2^{III}Zn_2^{II}(Ph\text{-}sao)_2(Ph\text{-}saoH)_4(hmp)_2]$ (**6**) and $[Mn_2^{III}(Naphth\text{-}sao)_2(Naphth\text{-}saoH)_2(MeOH)_2]$ (**7**) which are shown in Fig. 3 for comparison.[22] Although the bridging $[Mn(NO)]_2$ moiety remains the same in all seven complexes, com-

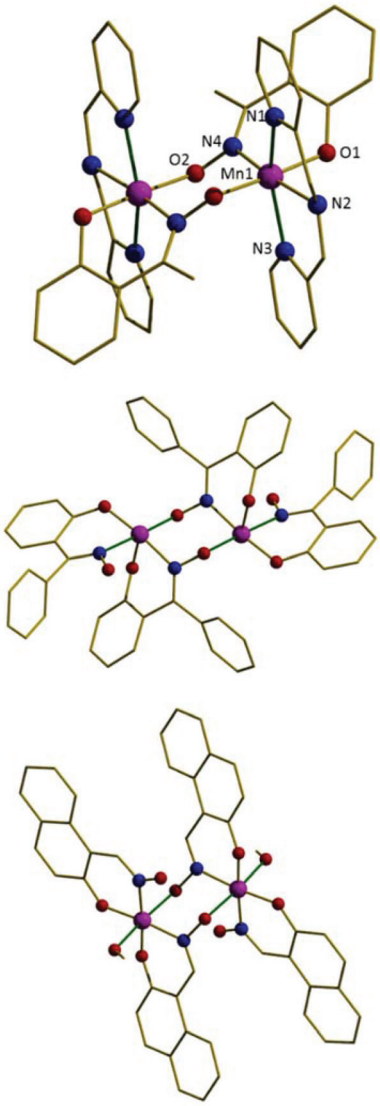

Fig. 3 The molecular structure of the cation of complex **2** (top), the magnetic core of complex **6** (middle), and complex **7** (bottom). The Jahn–Teller axes of the Mn^{III} ions are highlighted in dark green. Colour code: Mn = purple, O = red, N = blue, C = black. H-atoms are omitted for clarity.

Table 1 Summary of pertinent experimentally derived magneto-structural parameters for the $[Mn(NO)]_2$ family of complexes. Theoretically calculated J values for **1–6** are given in parantheses

Structure	Type	Mn–N–O–Mn torsion angle (°)	J (cm^{-1})
1	C	78.75	−5.73 (−5.76)
2	C	64.59	−3.63 (−2.16)
3	C	74.90	−5.63 (−5.15)
5	C	63.00	−2.05 (−2.99)
6	B	75.21	+2.20 (+2.65)
7	B	80.28	+1.24

plexes **6** and **7** differ in that they have their Mn^{III} Jahn–Teller axes co-parallel and in the bridging plane (structure type **B**, Fig. 1).

SQUID magnetometry

Dc magnetic susceptibility measurements were performed on polycrystalline samples of **1–3** and **5** in the temperature range T = 5–300 K in an applied magnetic field of B = 0.1 T. The poor yield of complex **4** precluded measurement. The experimental results are shown in Fig. 4 in the form of $\chi_M T$ products *vs.* T, where χ_M is the molar magnetic susceptibility, along with the data for complexes **6** and **7**.[22] At the highest temperatures measured the $\chi_M T$ values for **1–3** and **5** are ~4.1, 4.7, 4.8 and 5.0 cm^3 K mol^{-1}, respectively, all somewhat lower than that expected for two non-interacting, high spin d^4 ions with g = 2 (6 cm^3 K mol^{-1}). Upon cooling the $\chi_M T$ products of each sample behave very similarly, slowly decreasing with decreasing temperature reaching values of ~0.2 (**1**), 0.7 (**2**), 0.2 (**3**) and 1.1 cm^3 K mol^{-1} (**5**) at T = 5 K, indicative of the presence of weak antiferromagnetic exchange between the two Mn^{III} ions. This is in stark contrast to that observed for complexes **6** and **7** which display weak ferromagnetic exchange, as discussed in the articles highlighted in ref. 22.

$$\hat{H} = \mu_B B \sum_i g_i \hat{S}_i - 2 \sum_{i,j<i} J_{ij} \hat{S}_i \hat{S}_j \quad (1)$$

The data can be fit (Fig. 4, Table 1) to the model described by isotropic spin-Hamiltonian (1), where the indices i and j refer to the two Mn^{III} centres, J is the isotropic exchange interaction parameter, $\hat{S}$ is a spin operator, μ_B is the Bohr magneton, B is the applied magnetic field vector and g = 1.98 is the g-factor of the Mn^{III} ions. The best-fit parameters are J = −5.73 cm^{-1} (**1**), −3.63 cm^{-1} (**2**), −5.63 cm^{-1} (**3**) and −2.05 cm^{-1} (**5**). The ground spin-state of all four complexes is a spin singlet (S = 0; energy *versus* spin state plots are given in the ESI, Fig. S6–S9†). This can be compared to the S = 4 ground states observed for complexes **6** and **7** resulting from exchange interactions of +2.20 and +1.24 cm^{-1}, respectively.[22] The difference between the magnetic behaviour of **1–3**, **5** and **6–7** is intriguing, particularly given they have the same $[Mn(NO)]_2$ magnetic core, and thus it would appear that the orientation of the Jahn–Teller axes is an important structural parameter. In order to examine this in more detail we have therefore turned to Density Functional Theory.

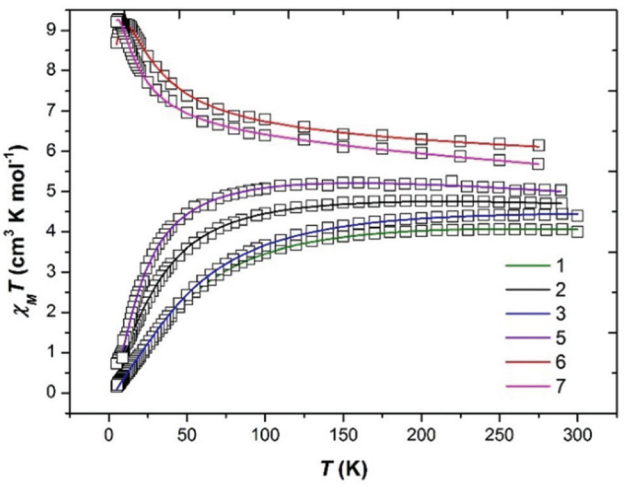

Fig. 4 Plot of the $\chi_M T$ product *versus* T for complexes **1–3**, **5–7**. The solid lines are a fit of the experimental data to isotropic spin-Hamiltonian (1). See text for details of the best fit parameters. Green = **1**, black = **2**, blue = **3**, purple = **5**, red = **6** and pink = **7**.

Theoretical studies

Theoretical studies have been carried out on complexes **1–6** in order to evaluate the exchange parameters and to reveal the mechanism of exchange. The DFT computed J values for complexes **1–6** are −5.76 cm^{-1}, −2.16 cm^{-1}, −5.15 cm^{-1}, −3.66 cm^{-1}, −2.99 cm^{-1} and +2.65 cm^{-1}, respectively (Table 1). Complexes **1–5** are found to exhibit weak antiferromagnetic exchange interactions, while complex **6** exhibits ferromagnetic exchange. Calculations reproduce not only the sign of J accurately but also their magnitude and the trend in magnitudes compared to that observed experimentally. To understand the electronic reasons behind the variation in the nature and magnitude of exchange and to analyse the effect of the relative orientation of the Jahn–Teller axes (structure types **B** and **C**), molecular orbitals (MO) and overlap integrals have been analysed for complexes **1–6**. The net exchange interaction in the dinuclear Mn^{III} moiety has two contributions: (i) an antiferromagnetic J_{AF} contribution arising solely from overlap between the singly occupied MOs (SOMOs) of the Mn^{III} ions, and (ii) a ferromagnetic J_F contribution arising from the orthogonality of the SOMOs (negligible overlap) and from the cross-interaction[22b,c] between the occupied and the empty d-orbitals (here between the $d_{x^2-y^2}$ and all the other Mn^{III} d-orbitals). Amongst the structures studied, the major contributor to the J_{AF} term is the overlap between the d_{xy} orbitals *via* the oxime bridge. This contribution is significant for complexes **1–5** possessing type **C** structures, as indicated in Fig. 1 and Fig. 5a. The second dominant contribution to the J_{AF} term is the d_{xz}–d_{xz} overlap, also

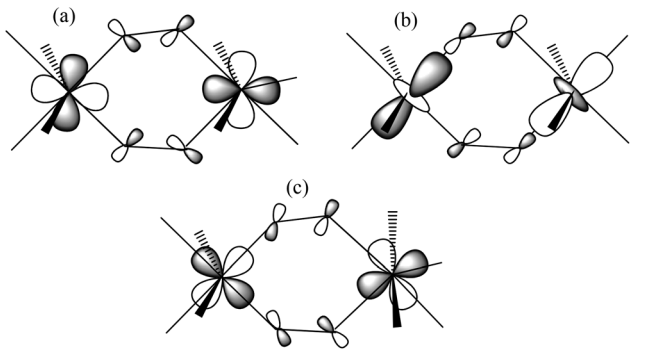

Fig. 5 Schematic representation of the (a) d_{xy}–d_{xy} overlap in complexes **1–5**, (b) d_{z^2}–d_{z^2} overlap in complex **6**, (c) cross-interaction between $d_{x^2-y^2}$ and d_{xz} in complexes **1–6**.

routed through the Mn–N–O–Mn bridge. Thus for complexes **1–5** the Mn–N–O–Mn torsion angle clearly dictates the strength of orbital overlap and thus the *J* value. These two overlaps are expected to be minimal in complex **6**, resulting in a very small J_{AF} term. However as the Jahn–Teller axes are now oriented along the oxime bridges, this allows for efficient d_{z^2}–d_{z^2} overlap (see Fig. 5b). In this scenario this latter overlap is dominant and this contributes to the J_{AF} term. As shown in Fig. 5b, this overlap is also strongly dependent upon the Mn–N–O–Mn torsion angle, with negligible overlap expected when the torsion angle approaches zero. Apart from these three prominent interactions, other orbital overlap values are small suggesting orthogonality between the SOMOs and a contribution to the J_F term. Along with moderate cross-interactions ($d_{x^2-y^2}$–d_{xz}) this leads to a significant J_F term for all complexes **1–6**. The sign of *J* in each case is dictated by the dominant factor; for **1–5** the two strong overlaps overwhelmingly dominate leading to net antiferromagnetic exchange, while the prominent d_{z^2}–d_{z^2} overlap observed in complex **6** is overshadowed by the J_F contributions leading to a net ferromagnetic interaction.

Spin density plots were computed in order to understand the origin of the electronic differences in complexes **1–6**. Unpaired electrons in t_{2g} orbitals usually favour a spin polarisation mechanism, whereas those in the e_g orbitals tend to facilitate a spin delocalisation mechanism. In the case of the Mn^{III} ion a mixture of these two mechanisms is found to operate since the ion possesses three unpaired electrons in the t_{2g} orbitals and one unpaired electron in the e_g orbital. The spin density of the Mn^{III} ions in **1–6** is found to be <3.8 which shows that it is centred on the metal ion with a dominant spin delocalisation mechanism. The bridging N and O spin densities are different for the two structure types studied; for complex **1** all the bridging N and O atoms possess negative spin density indicating spin polarisation, while complex **6** possesses positive spin density on the O atom due to spin delocalistion as it lies along the Jahn–Teller axis (see Table S8 in ESI† and Fig. 6) and negative spin density on the N atom due to spin polarisation.

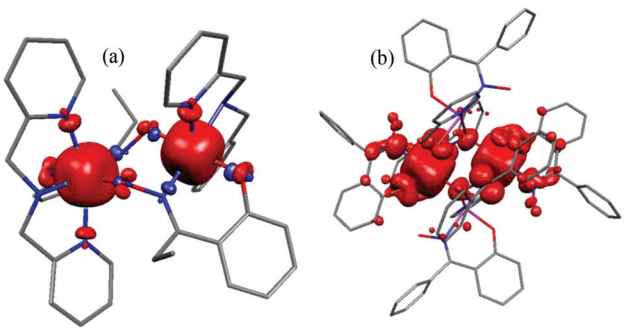

Fig. 6 Computed spin density HS plot for complex **1** (a) and complex **6** (b).

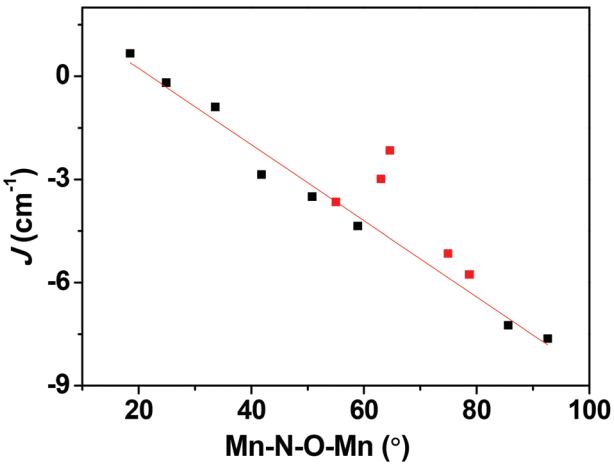

Fig. 7 Magneto-structural correlations developed by varying the Mn–N–O–Mn dihedral angle in **1**. The red squares are experimental *J* values obtained for complexes **1–5**.

Apart from the orientation of the Jahn–Teller axis, the Mn–N–O–Mn torsion angle also plays a role in dictating the sign and magnitude of the *J* values. To see if it is possible to obtain ferromagnetic coupling in type **C** structures, we have developed magneto-structural correlations by varying the Mn–N–O–Mn dihedral angle from 18.5 to 92.8° in complex **1**. A plot of *J versus* Mn–N–O–Mn dihedral angle is shown in Fig. 7. Our correlation reveals that *J* switches its sign from antiferromagnetic to ferromagnetic with decreasing dihedral angle. As the torsion angle decreases, the cross-interaction between $d_{x^2-y^2}$ and d_{xz}/d_{xy} strengthens, leading to a larger J_F contribution which in turn results in ferromagnetic exchange. Our calculations predict that a more planar Mn–N–O–Mn moiety of structure type **C** will exhibit ferromagnetic exchange coupling. Synthetic efforts to produce such a molecule are underway in our laboratory.

Conclusions

The simple reaction between a Mn salt, a phenolic oxime and the tridentate chelate dpa affords a small family of double-oxime bridged Mn^{III} dimers, whose structures differ from previous examples in the orientation of their Jahn–Teller axes. Previous family members conform to structure type **B** with the JT axes co-parallel and in the bridging plane between the Mn^{III} ions, resulting in ferromagnetic exchange. The addition of a chelating ligand results in the novel complexes **1–5** whose JT axes have now switched orientation giving structure type **C**, where they lie perpendicular to the $[Mn(ON)]_2$ bridging plane. The result is that the magnetic exchange between the metal centres becomes weakly antiferromagnetic. The employed DFT methodology is able to reproduce both the sign and magnitude of the exchange interaction in complexes **1–6**. MO analysis reveals two dominant overlaps between the d_{xy}–d_{xy} and d_{xz}–d_{xz} orbitals are found to control the sign and magnitude of

exchange in complexes **1–5**. In the case of complex **6**, strong d_{z^2}–d_{z^2} overlap is overcome by cross-interactions and orbital orthogonality resulting in a weak ferromagnetic interaction. The general mechanism of exchange proposed can, in principle, be extended to any double oxime bridged Mn^{III} dimer. Our developed magneto-structural correlation suggests a switch in the sign of the exchange interaction from antiferromagnetic to ferromagnetic upon decreasing the Mn–N–O–Mn torsion angle to approximately 20°.

Acknowledgements

GR thanks the DST (EMR/2014/000247), DST Nanomission and INSA for funding. TR thanks the CSIR for a SRF fellowship.

Notes and references

1 D. Gatteschi, R. Sessoli and J. Villain, *Molecular Nanomagnets*, Oxford University Press, Oxford, U.K., 2006.
2 J. M. Clemente-Juan, E. Coronado and A. Gaita-Ariño, *Chem. Soc. Rev.*, 2012, **41**, 7464.
3 L. Bogani and W. Wernsdorfer, *Nat. Mater.*, 2008, **7**, 179.
4 M. N. Leuenberger and D. Loss, *Nature*, 2001, **410**, 789.
5 M. Evangelisti, in *Molecular Magnets, NanoScience and Technology*, ed. J. Bartolomé, F. Luis and J. F. Fernández, Springer-Verlag, Berlin, Heidelberg, 2014, pp. 365–387.
6 (*a*) G. Aromí and E. K. Brechin, *Struct. Bonding*, 2006, **122**, 1; (*b*) C. J. Milios and R. E. P. Winpenny, *Struct. Bonding*, 2015, **164**, 1.
7 W. Wernsdorfer and R. Sessoli, *Science*, 1999, **284**, 133.
8 S. Thiele, F. Balestro, R. Ballou, S. Klyatskaya, M. Ruben and W. Wernsdorfer, *Science*, 2014, **344**, 1135.
9 M. Ganzhorn, S. Klyatskaya, M. Ruben and W. Wernsdorfer, *Nat. Nanotechnol.*, 2013, **8**, 165.
10 M. Urdampilleta, S. Klyatskaya, J.-P. Cleuziou, M. Ruben and W. Wernsdorfer, *Nat. Mater.*, 2011, **10**, 502.
11 J.-P. Cleuziou, W. Wernsdorfer, V. Bouchiat, T. Ondarçuhu and M. Monthioux, *Nat. Nanotechnol.*, 2006, **1**, 53.
12 M. Baker, T. Guidi, S. Carretta, J. Ollivier, H. Mutka, H.-U. Güdel, G. A. Timco, E. J. L. McInnes, G. Amoretti and R. E. P. Winpenny, *Nat. Phys.*, 2012, **8**, 906.
13 S. Hill, R. S. Edwards, N. Aliaga-Alcalde and G. Christou, *Science*, 2003, **302**, 1015.
14 W. Wernsdorfer, N. Aliaga-Alcalde, D. N. Hendrickson and G. Christou, *Nature*, 2002, **416**, 406.
15 J. D. Rinehart, M. Fang, W. J. Evans and J. R. Long, *J. Am. Chem. Soc.*, 2011, **133**, 14236.
16 S. Loth, S. Baumann, C. P. Lutz, D. M. Eigler and A. J. Heinrich, *Science*, 2012, **335**, 196.
17 (*a*) M. Evangelisti, A. Candini, A. Ghirri, M. Affronte, E. K. Brechin and E. J. L. McInnes, *Appl. Phys. Lett.*, 2005, **87**, 072504; (*b*) M. Evangelisti and E. K. Brechin, *Dalton Trans.*, 2010, **39**, 4672; (*c*) K. R. Vignesh, S. K. Langley, K. S. Murray and G. Rajaraman, *Chem. – Eur. J.*, 2015, **21**, 2881.
18 M. Mannini, F. Pineider, C. Danielli, F. Totti, L. Sorace, P. Sainctavit, M.-A. Arrio, E. Otero, L. Joly, J. C. Cezar, A. Cornia and R. Sessoli, *Nature*, 2010, **468**, 417.
19 J. Lehmann, A. Gaita-Ariño, E. Coronado and D. Loss, *Nat. Nanotechnol.*, 2007, **2**, 312.
20 (*a*) J. Liu and S. Hill, *Polyhedron*, 2013, **66**, 147; (*b*) S. Hill, S. Datta, J. Liu, R. Inglis, C. J. Milios, P. L. Feng, J. J. Henderson, E. del Barco, E. K. Brechin and D. N. Hendrickson, *Dalton Trans.*, 2010, **39**, 4693.
21 D. Gatteschi, O. Kahn and R. D. Willet, *Magneto-Structural Correlations in Exchange-Coupled Systems*, D. Reidel, Dordrecht, 1985.
22 (*a*) D. A. Pantazis, V. Krewald, M. Orio and F. Neese, *Dalton Trans.*, 2010, **39**, 4959; (*b*) N. Berg, T. Rajeshkumar, S. M. Taylor, E. K. Brechin, G. Rajaraman and L. F. Jones, *Chem. – Eur. J.*, 2012, **18**, 5906; (*c*) W. P. Barros, R. Inglis, G. S. Nichol, T. Rajeshkumar, G. Rajaraman, S. Piligkos, H. O. Stumpf and E. K. Brechin, *Dalton Trans.*, 2013, **42**, 16510; (*d*) R. Inglis, E. Houton, J. Liu, A. Prescimone, J. Cano, S. Piligkos, S. Hill, L. F. Jones and E. K. Brechin, *Dalton Trans.*, 2011, **40**, 9999; (*e*) E. Houton, S. M. Taylor, C. C. Beedle, J. Cano, S. Piligkos, S. Hill, A. G. Ryder, E. K. Brechin and L. F. Jones, *Dalton Trans.*, 2012, **41**, 8340.
23 C. J. Milios, R. Inglis, L. F. Jones, S. Piligkos and E. K. Brechin, *Chem. Commun.*, 2012, **48**, 181; C. J. Milios, S. Piligkos and E. K. Brechin, *Dalton Trans.*, 2008, 1809.
24 W. R. Dunstan and T. A. Henry, *J. Chem Soc., Trans.*, 1899, **75**, 66.
25 (*a*) G. M. Sheldrick, *Acta Crystallogr., Sect. A: Found. Crystallogr.*, 2008, **64**, 112; (*b*) O. V. Dolomanov, L. J. Bourhis, R. J. Gildea, J. A. K. Howard and H. Puschmann, *J. Appl. Crystallogr.*, 2009, **42**, 339; (*c*) L. Palatinus and G. Chapuis, Superflip - a computer program for the solution of crystal structures by charge flipping in arbitrary dimensions, *J. Appl. Crystallogr.*, 2007, **40**, 786–790.
26 A. D. Becke, *J. Chem. Phys.*, 1993, **98**, 5648.
27 (*a*) A. Schafer, H. Horn and R. Ahlrichs, *J. Chem. Phys.*, 1992, **97**, 2571; (*b*) A. Schafer, C. Huber and R. Ahlrichs, *J. Chem. Phys.*, 1994, **100**, 5829.
28 M. J. Frisch, G. W. Trucks, H. B. Schlegel, G. E. Scuseria, M. A. Robb, J. R. Cheeseman, G. Scalmani, V. Barone, B. Mennucci, G. A. Petersson, H. Nakatsuji, M. Caricato, X. Li, H. P. Hratchian, A. F. Izmaylov, J. Bloino, G. Zheng, J. L. Sonnenberg, M. Hada, M. Ehara, K. Toyota, R. Fukuda, J. Hasegawa, M. Ishida, T. Nakajima, Y. Honda, O. Kitao, H. Nakai, T. Vreven, J. A. Montgomery Jr., J. E. Peralta, F. Ogliaro, M. Bearpark, J. J. Heyd, E. Brothers, K. N. Kudin, V. N. Staroverov, R. Kobayashi, J. Normand, K. Raghavachari, A. Rendell, J. C. Burant, S. S. Iyengar, J. Tomasi, M. Cossi, N. Rega, J. M. Millam, M. Klene, J. E. Knox, J. B. Cross, V. Bakken, C. Adamo, J. Jaramillo, R. Gomperts, R. E. Stratmann, O. Yazyev, A. J. Austin, R. Cammi, C. Pomelli, J. W. Ochterski, R. L. Martin, K. Morokuma, V. G. Zakrzewski, G. A. Voth, P. Salvador,

J. J. Dannenberg, S. Dapprich, A. D. Daniels, O. Farkas, J. B. Foresman, J. V. Ortiz, J. Cioslowski and D. J. Fox, *GAUSSIAN 09 (Revision A.02)*, Gaussian, Inc., Wallingford, CT, 2009.

29 L. Noodleman, *J. Chem. Phys.*, 1981, **74**, 5737.

30 (*a*) E. Ruiz, S. Alvarez, J. Cano and P. Alemany, *J. Comput. Chem.*, 1999, **20**, 1391; (*b*) E. Ruiz, A. Rodriguez-Fortea, J. Cano, S. Alvarez and P. Alemany, *J. Comput. Chem.*, 2003, **24**, 982; (*c*) G. Rajaraman, J. Cano, E. K. Brechin and E. J. L. McInnes, *Chem. Commun.*, 2004, 1476; (*d*) P. Christian, G. Rajaraman, A. Harrison, J. J. W. McDouall, J. Raftery and R. E. P. Winpenny, *Dalton Trans.*, 2004, 2550; (*e*) G. Rajaraman, M. Murugesu, E. C. Sanudo, M. Soler, W. Wernsdorfer, M. Helliwell, C. Muryn, J. Raftery, S. J. Teat, G. Christou and E. K. Brechin, *J. Am. Chem. Soc.*, 2004, **126**, 15445; (*f*) S. Sasmal, S. Hazra, P. Kundu, S. Dutta, G. Rajaraman, E. C. Sañudo and S. Mohanta, *Inorg. Chem.*, 2011, **50**, 7257; (*g*) L. F. Jones, G. Rajaraman, J. Brockman, M. Murugesu, J. Raftrey, S. J. Teat, W. Wernsdorfer, G. Christou, E. K. Brechin and D. Collison, *Chem. – Eur. J.*, 2004, **10**, 5180.